

# Modeling Study of Cyclic Oxidation Behavior of NiAl and NiCr Alloys

X.J. Peng, K.Y. Chen, R. Liu, and M. Liang

(Submitted July 24, 2014; in revised form September 1, 2014; published online September 23, 2014)

The cyclic oxidation behavior of four high-temperature alloys (two NiAl alloys and two NiCr alloy) is studied utilizing an existing micromechanics-based model, in which  $\text{Al}_2\text{O}_3$  and  $\text{Cr}_2\text{O}_3$  are formed on the alloys as protective layers. For each alloy, the model parameters are determined based on one ‘complete’ experimental curve of weight change, which is obtained under a high-temperature cyclic oxidation test where the weight change experiences a maximum value and then drops down to a zero point. The model is first tested on two metals which have experimental data available for comparison. It is found that the model parameter, oxide crack density exponent, can be assumed constant within a range of high temperature for each metal, thus with the ‘complete’ experimental curve of weight change, the model can predict the oxidation behavior of the metal at different temperatures. The determination of model parameters, accuracy, and limitations of the model for NiAl and NiCr alloys is analyzed and discussed.

**Keywords** modeling and simulation, oxidation, superalloys

## 1. Introduction

Protective coating is crucial for preventing high-temperature alloy substrate from cyclic oxidation degradation. Various coatings, such as NiCrAlY, CoCrAlY, and NiAl<sub>2</sub>O<sub>3</sub>, have been developed to protect the high-temperature structural alloys (Ref 1-6). The oxidation resistance of most protective coatings is attributed to their adherent and continuous oxide layer, e.g., aluminum-contained alloys normally have excellent oxidation resistance at 1200 °C because of continuous formation of Al<sub>2</sub>O<sub>3</sub> film (Ref 7, 8). However, due to the change in service environment, the oxide film may not remain on the alloy surface. At high temperatures, the thermal cycling can induce oxide film, but during cooling cycle, the oxide film may spall off from the surface. As a result, the thickness of the oxide layer will decrease (Ref 9, 10), and this in turn increases the oxidation rate of the substrates, thus the coating life would decrease significantly (Ref 11). To study the cyclic oxidation behavior and predict the service life of the protective coatings, the interaction between oxidation and spallation must be investigated.

There are two modes of oxide spallation according to stress condition (Ref 12-18). For tensile stress case, micro-cracks are easily formed in the oxide layer but less spallation would occur because of insufficient shear stresses. In compressive stress case, depending on the interface strength, the oxide spallation is

considered as either a wedging process or a bulking process. Robertson and Manning (Ref 12) investigated the failure of oxide scales under rapidly applied strains, assuming that no relaxation occurred. Their work was the extension of the semi-empirical study of Armitt et al. (Ref 19), which showed that failure occurred when the elastic strain built up in the oxide until the strain energy density exceeded the surface fracture energy of the oxide. They developed the failure mode maps which related failure strain to oxide thickness. Hancock and Nicholls (Ref 15) studied the mechanisms of scale fracture due to stresses generated during growth, applied directly or by thermal cycling, including the influence of defects in the scale on fracture toughness. The mechanical behavior of the oxide scale over a wide range of operating conditions could be predicted by comparing the yield and fracture behavior of the scale. Evans (Ref 16) investigated the effect of temperature change on the strains developed between oxide and substrate and found that temperature change posed a significant threat to the integrity of protective-oxide layers because of the differential strains developed between oxide and substrate, because it may induce either tensile or compressive in-plane stresses within the oxide layer. The former may produce cracks through the thickness of this layer but oxide spallation under such tensile conditions appeared to be a difficult process. By contrast, spallation was relatively easy under compression, i.e., in most cases during cooling from the oxidation temperature.

However, the deficiency of above research was obvious, because all the methods developed in the research were unable to predict the failure and service life of a coating under cyclic oxidation. Probst and Lowell (Ref 20) and Lowell et al. (Ref 21) developed the cyclic oxidation spalling program (COSP), which was a model allowing the prediction of cyclic oxidation at the peak temperature and spallation during cool down, over a wide range of exposure condition (temperature). Furthermore, the failure mechanism of the oxides on nickel based alloys during cyclic oxidation was investigated based on a degradation model combined with oxide formation simulation (Ref 22); the

X.J. Peng and M. Liang, and Department of Mechanical Engineering, University of Ottawa, 770 King Edward Avenue, Ottawa, ON K1N 6N5, Canada; K.Y. Chen, Aerospace Portfolio, National Research Council of Canada, 1200 Montreal Road, Ottawa, ON, Canada K1A 0R6; and R. Liu, Department of Mechanical and Aerospace Engineering, Carleton University, 1125 Colonel By Drive, Ottawa, ON K1S 5B6, Canada. Contact e-mail: Rong.Liu@carleton.ca.

life of the oxides during the cyclic process could be predicted using this model. Based on these concepts, Chan (Ref 23) proposed a micromechanics-based model simulating spallation of an oxide scale on a coated metallic substrate when subjected to a cooling down cycle with a temperature change. This model requires a group of parameters for each alloy that must be determined via a cyclic oxidation test at a high temperature where a 'complete' weight change curve that has a maximum value and then a drop trend down to a zero point can be obtained. Up to date, only limited metals have been studied as a comparison baseline of the Chan's model, and therefore, to explore the predictability of this model, further study of this model on more metals, such as  $\text{Al}_2\text{O}_3$  and  $\text{Cr}_2\text{O}_3$  grown on different types of alloy, is necessary.

In this research, the cyclic oxidation behavior of two NiAl alloys and two NiCr alloys was studied using the Chan's model. Based on the available experimental data (Ref 24) for these alloys, the simulation was performed at the temperatures between 1050 and 1200 °C, in order to compare the predicted weight changes with the experimental measurements. The growth and spallation behavior of  $\text{Al}_2\text{O}_3$  and  $\text{Cr}_2\text{O}_3$  scales on these alloys were investigated. The plots of the oxide weight change versus exposing time were obtained for the alloys. The model parameters, simulation results, and limitations of the model were essentially discussed.

## 2. Cyclic Oxidation Modeling

### 2.1 Oxidation and Spallation Models

Cyclic oxidation process comprises both oxidation and spallation steps. In high-temperature environments, metallic substances are much easier to be oxidized than at room temperature. They count on the protective coatings to provide the oxidation resistance. Most of these coatings are an adherent and continuous oxide layer. The layer can isolate substrate from air; resultantly, the reaction between the substrate, metallic elements in the coating, and oxygen can be limited. However, during thermal cycling, the oxide layer may become discontinuous as the depletion of the oxide-forming metallic elements in the coating. The COSP is one of the cyclic oxidation models. The oxidation at the peak temperature of a thermal cycle as the basis of the COSP can be expressed as (Ref 20, 21)

$$W_{\text{ox}} = Z\sqrt{k_p t}, \quad (\text{Eq 1})$$

where  $W_{\text{ox}}$  is the weight of the oxide formed,  $t$  is the time of oxidation for one cycle,  $Z$  is the ratio of the molecular weight of the oxide to the molecular weight of oxygen, and  $k_p$  is the parabolic rate constant.

The decohesion occurs in the oxide or at the interface and fracture are found on the planes within the oxide. Utilizing the COSP model, the spallation of the oxide is represented in terms of an empirical relation (Ref 20, 21)

$$f = Q_0(W_{\text{ox}})^\gamma, \quad (\text{Eq 2})$$

where  $f$  is the fraction of oxide spalled,  $Q_0$  is the proportional constant, and  $\gamma$  is an exponent. With some experimental data, Eq 1 and 2 can be used to calculate some weights or weight changes, such as weight of oxide remained on the

metal surface,  $W_p$ , weight of oxide spalled,  $W_s$ , weight change,  $W_c$ , and weight loss of oxide-forming elements,  $W_m$ , which are necessary parameters used for predicting failure of the oxide.

Spallation of an oxide scale on a coated metallic substrate occurs during a cooling cycle with a temperature change. In the Chan's model (Ref 23), the height and width of the substrate are  $H$  and  $B$ , respectively, as shown in Fig. 1(a), and the thickness of the oxide is  $b$ , as indicated in Fig. 1(b). The oxide scale is subjected to a compressive stress,  $\sigma_c$ , which is composed of an applied stress,  $\sigma_\infty$ , and a thermal stress induced due to a mismatch in the thermal expansion coefficients between the oxide and the metal. The oxide scale is assumed to contain a number of preexisting shear cracks created by the growth stress and the thermal stresses during the cooling process (Ref 13). The average length of the shear cracks on the oxide surface is  $2a$ , as shown in Fig. 1(a) and the initial average crack depth is  $l_0$ , which is not normal to the oxide surface, but has an angle,  $\psi$  with the surface normal, see Fig. 1(b), thus the projected length of the shear crack on the normal plane is  $l_0 \sin \psi$ , as depicted in Fig. 1(c). When subjected to the compressive stress, some of the shear cracks develop into wing tips with a length,  $l$ , which propagate in a direction parallel to the compressive stress direction or the oxide surface, as illustrated in Fig. 1(b) (Ref 25, 26). A spall is formed and becomes detached from the scale when the wing crack joins with an adjacent shear crack; the volume of a spall formed in the oxide layer is illustrated in Fig. 1(c). At the micromechanics scale, the weight of spalled oxide is (Ref 20, 21)

$$W_s = \rho_{\text{ox}} v_s n_c / 2, \quad (\text{Eq 3})$$

where  $\rho_{\text{ox}}$  is the density of the oxide,  $v_s$  is the unit volume of an oxide spall, and  $n_c$  is the number of shear cracks with wing tips. The unit volume of a spall is expressed as

$$v_s = 2al_0 \sin \psi, \quad (\text{Eq 4})$$

where  $\psi$  is the angle between the direction of the compressive stress and shear crack,  $a$  is the average half-length of shear crack, and  $l_0$  is the initial average depth of shear crack. The density,  $\rho_{\text{ox}}$ , is given by

$$\rho_{\text{ox}} = \frac{W_{\text{ox}}}{BHh}, \quad (\text{Eq 5})$$

where  $B$  and  $H$  are the oxide dimensions and  $h$  is the oxide thickness. Eq 3 to 5 lead to

$$W_s = \xi L (\sin \psi) W_{\text{ox}}, \quad (\text{Eq 6})$$

where  $\xi = \frac{n_c a l_0^2}{BHh}$  is the normalized crack density and  $L = \frac{l}{l_0}$  is the ratio of wing crack depth to shear crack depth. Equation 6 requires the crack parameters for the model, which are difficult to obtain experimentally; therefore, Chan (Ref 23) proposed a more convenient expression for  $W_s$  as

$$W_s = q \Delta T^2 \left( \frac{W_{\text{ox}}}{W_0} \right)^{1+m}, \quad (\text{Eq 7})$$

where  $q$  and  $m$  are spallation and crack density constants of the oxide, respectively;  $\Delta T$  is temperature change;  $W_0$  is the reference weight and is taken as 1 mg/cm<sup>2</sup> for convenience. Based on the above discussion, it is easy to get the following relationship:

$$W_r = W_{ox} - W_s \quad (\text{Eq 8})$$

Since cyclic oxidation is time dependent, the cumulative weight change, the entire weight of spallation, and the weight of the metal element loss are a function of cycle time. The equation for the cumulative oxide weight change per unit area after  $n$ th cycles is (Ref 23):

$$(W_c)_n = (1/Z)(W_r)_n - (1 - 1/Z) \left( \sum_1^n W_s \right) \quad (\text{Eq 9})$$

$W_r$  can be calculated by  $W_s$  and  $W_{ox}$  from Eq 8.  $W_s$  and  $W_{ox}$  are given by Eq 1 and 7, respectively.

## 2.2 Parameters of the Model

In the cyclic oxidation simulation, combining Eq 1, 7 to 9 yields the following equation

$$(W_c)_n = (1/Z) \left[ Z\sqrt{k_p t} - q\Delta T^2 \left( \frac{Z\sqrt{k_p t}}{W_o} \right)^{1+m} \right]_n - (1 - 1/Z) \left[ \sum_1^n q\Delta T^2 \left( \frac{Z\sqrt{k_p t}}{W_o} \right)^{1+m} \right]_n \quad (\text{Eq 10})$$

In Eq 10, parameters  $Z$ ,  $K_p$ ,  $m$ , and  $q$  must be determined before the weight change with oxidation cycle can be obtained.  $Z$  is the ratio of the molecular weight of the oxide to the molecular weight of oxygen in the oxide. For  $\text{Al}_2\text{O}_3$ ,  $Z = (16 \times 3 + 27 \times 2)/(16 \times 3) = 2.125$ . For  $\text{Cr}_2\text{O}_3$ ,  $Z = (16 \times 3 + 52 \times 2)/(16 \times 3) = 3.167$ .  $K_p$  is the parabolic rate constant of oxide growth, which varies with type of oxide and temperature under oxidation. The value of  $K_p$  can be

determined experimentally for various alloys under different oxidation temperatures.

The crack density exponent  $m$  (Ref 23) is related to the properties of the oxide scale. Different values of  $m$  indicate different physical meanings. For  $m = 0$ , it means that the density of cleavage wing cracks and the oxide thickness are independent, i.e., the spallation occurs at the oxide/substrate interface. For  $m > 0$ , bulk spallation takes place on the planes within the oxide. This implies that not all cleavage wing cracks lie on the interface plane for complete interface decohesion. The value of  $m$  can be determined experimentally by measuring the rate of weight change of the material under cyclic oxidation, as expressed by the following equation (Ref 23)

$$m = \frac{-2}{\lg\left(\frac{t_m}{t_s}\right)} \lg \left[ \frac{-2t_m \dot{W}_c}{(1 - 1/Z)\sqrt{k_p t_s}} \right], \quad (\text{Eq 11})$$

where  $t_m$  is the time when weight change curve reaches the maximum,  $t_s$  is the time when net weight change is zero.  $\dot{W}_c$  is the rate of weight change at the steady state, which can be obtained from the weight change curve. The spallation constant  $q$  is influenced by the cracks in the oxide layers, such as the crack length, fracture toughness, and density (Ref 23). The value of  $q$  is related to the value of  $m$ , expressed as

$$q = \frac{t}{2Zt_m\Delta T^2} \left( 1 + \frac{t}{2t_m} \right)^{-(1+m)} \left( \frac{W_o}{Z\sqrt{k_p t_m}} \right)^m. \quad (\text{Eq 12})$$

## 2.3 Validation of Cyclic Oxidation Model

To verify the Chan's model, the cyclic oxidation behavior of an austenitic stainless steel (Fe-Ni-Cr-Al) and a Ni-based alloy (Ni-48.3Al-0.1Zr) at temperatures between 1200 and 1000 °C was investigated. The values of parameters  $m$  and  $q$  used in the simulations were determined from the experimental fitting curves that were obtained in the cyclic oxidation tests at the highest temperature (1200 °C) within the temperatures under test (Ref 27, 28), because at this temperature with less cycles or within shorter time, a "complete" weight change curve, which has a maximum value and then a drop trend down to a zero point, could be derived from the tests for Fe-Ni-Cr-Al and Ni-48.3Al-0.1Zr, respectively. The final parameters used in the simulation for Fe-Ni-Cr-Al and Ni-48.3Al-0.1Zr are summarized in Table 1 (Ref 23). The oxide weight  $W_{ox}$  was calculated from Eq 1. The weight of spalled oxide  $W_s$  was calculated from Eq 7. Thus, the weight of residual oxide  $W_r$  was obtained from Eq 8.  $W_s$  and  $W_r$  were calculated in weight per unit area. Finally, the cumulative weight changes of oxide per unit area after  $n$ th cycles for Fe-Ni-Cr-Al at 1200, 1100, and 1000 °C and for Ni-48.3Al-0.1Zr at 1200, 1150, and 1100 °C were calculated using the  $m$  and  $q$  values determined at  $T = 1200$  °C; the results are plotted in Fig. 2 and 3, together with the experimental data (Ref 27, 28) for comparison.

It is observed that although theoretically the values of parameters  $m$  and  $q$  vary with temperature, as demonstrated by Eq 11 and 12, the predicted weight changes using the same values of  $m$  and  $q$  for the temperature range between 1000 and 1200 °C show good agreement with the experimental measurements. Regarding the cyclic oxidation versus temperature, for both of the materials, at 1200 °C oxidation, oxide weight change increases with the number of cycle initially, but after about 25 cycles for Fe-Ni-Cr-Al and 600 cycles for

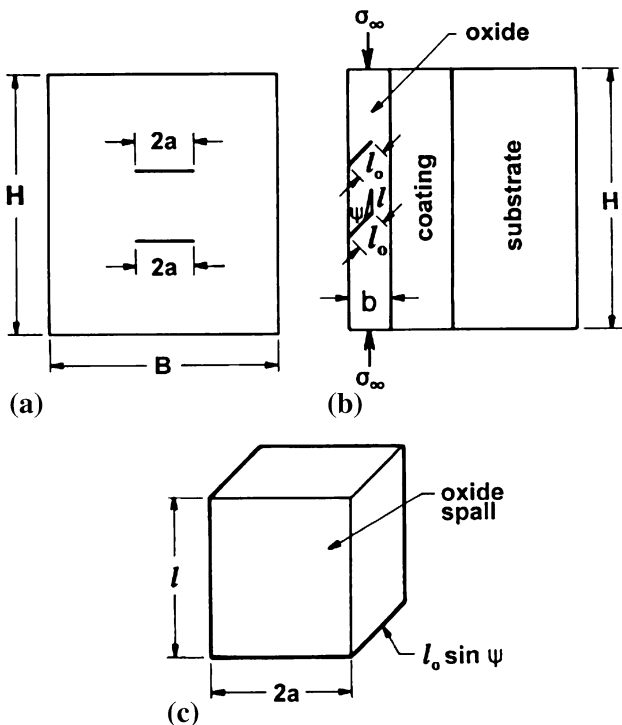


Fig. 1 Schematic drawing of an oxidized alloy surface (Ref 23)

**Table 1 Parameters used for the cyclic oxidation model validation (Ref 23)**

Material	$T_{max}$ , °C	$T_{min}$ , °C	$K_p$ , mg <sup>2</sup> /cm <sup>4</sup> /h	$q$ , mg/cm <sup>2</sup> /°C <sup>2</sup>	$m$	$Z$	$t$ , h
Fe-Ni-Cr-Al	1200	25	$1.1 \times 10^{-2}$	$8 \times 10^{-11}$	3	2.125	20
	1100	25	$8.0 \times 10^{-4}$	$8 \times 10^{-11}$	3	2.125	20
	1000	25	$8.65 \times 10^{-5}$	$8 \times 10^{-11}$	3	2.125	20
Ni-48.3Al-0.1Zr	1200	60	$1.51 \times 10^{-2}$	$1.2 \times 10^{-11}$	1	2.125	1
	1150	60	$6.62 \times 10^{-3}$	$1.2 \times 10^{-11}$	1	2.125	1
	1100	60	$2.31 \times 10^{-3}$	$1.2 \times 10^{-11}$	1	2.125	1

Ni-48.3Al-0.1Zr, it decreases straightly, indicating significant spallation of oxide scales. Also, within the low cycles (45 cycles for Fe-Ni-Cr-Al alloy steel and 400 cycles for Ni-48.3Al-0.1Zr alloy), the theoretical simulations well fit the experimental data; the error is less than 5%, but the model prediction for the high cycles seems not very accurate with respect to the experimental observation. At the lower temperatures (1000-1100 °C), oxide weight change increases continuously with the number of cycle, representing unceasing growth of the oxide scales. To investigate the degradation behavior of the oxides and coating's life at these temperatures, the cyclic oxidation test must be performed for more cycles or longer time, which is time consuming and costly. The simulation results well predict the oxidation behavior of the materials at these temperatures, with the average error about 10%.

### 3. Cyclic Oxidation of NiAl and NiCr Alloys

#### 3.1 Determination of Model Parameters

To explore to the predictability of the model for the Al<sub>2</sub>O<sub>3</sub> scales formed on the substrates with other compositions and also to examine if the model can be applicable for Cr<sub>2</sub>O<sub>3</sub> scales, four alloys: Ni-48Al-0.1Zr, NiAl, DH-245, and Ni30Cr, were studied using the Chan's model. The chemical composition of these alloys is given in Table 2. The selection of these alloys was also because the experimental data for them were available (Ref 24). Ni-48Al-0.1Zr and NiAl were tested for Al<sub>2</sub>O<sub>3</sub> as the protective scale but on different substrates, while DH-245 and Ni-30Cr were for Cr<sub>2</sub>O<sub>3</sub> as the protective scale.

For Ni-48Al-0.1Zr and NiAl, the oxide is Al<sub>2</sub>O<sub>3</sub>, then  $Z = (16 \times 3 + 27 \times 2)/(16 \times 3) = 2.125$ .

For DH-245 and Ni-30Cr, the oxide is Cr<sub>2</sub>O<sub>3</sub>, then  $Z = (16 \times 3 + 52 \times 2)/(16 \times 3) = 3.167$ .

The initially calculated  $m$  values from the fitting curves using Eq 11 are given in Table 3. To achieve the best simulating results with respect to the experimental data, these  $m$  values were revised through trial-and-errors procedure, and the revised  $m$  values are also presented in Table 3. The other model parameters required in the simulation are summarized in Table 4; the  $q$  values were calculated using Eq 12 with the revised  $m$  values; the  $K_p$  values were obtained by Smialek et al. (Ref 24).

#### 3.2 Growth and Degradation Behavior of Al<sub>2</sub>O<sub>3</sub> and Cr<sub>2</sub>O<sub>3</sub>

With the revised  $m$  and  $q$  values, the simulation results of the NiAl alloys are plotted in Fig. 4 and 5, along with the experimental data (Ref 24) for comparison. It can be seen that,

in general, the modeling results agree well with the experimental data, in particular, in the low cycle range with the average error about 3.5%. However, after 1500 cycles, the model predictions overestimate the weight changes, compared with the experimental data. At the high temperature (1200 °C), the Al<sub>2</sub>O<sub>3</sub> scales grow rapidly at the initial stage and reach the maximum (about 2.2 mg/cm<sup>2</sup> for Ni-48Al-0.1Zr and 1.65 mg/cm<sup>2</sup> for NiAl) at 500 cycles, and then degrade gradually with the oxidation cycle. After 2500 cycles of oxidation, the weight changes of the two NiAl alloys resume to zero, which implies that the Al<sub>2</sub>O<sub>3</sub> scales have totally spalled from the surface of the alloys.

The variations of weight change with oxidation cycle for the NiCr alloys are illustrated in Fig. 6 and 7, together with the experimental data (Ref 24) for comparison. Different from the NiAl alloys, the Cr<sub>2</sub>O<sub>3</sub> scales on DH-245 at 1150 °C and on Ni30Cr at 1050 °C grow to the maximum (about 1.2 mg/cm<sup>2</sup> for DH-245 and 0.35 mg/cm<sup>2</sup> for Ni30Cr) at much less oxidation cycles (around 40 cycles for DH-245 and 15 cycles for Ni30Cr). After that Cr<sub>2</sub>O<sub>3</sub> is continuously formed on the alloys, but accompanied by spallation of the oxides. The synergetic effect of formation and spallation of Cr<sub>2</sub>O<sub>3</sub> results in serious material loss of the alloys eventually, as illustrated in Fig. 6 and 7. The error of the model prediction for this alloy is averagely 4.6%.

Comparing the cyclic oxidation behavior between NiAl and NiCr alloys, it is found that Al<sub>2</sub>O<sub>3</sub> is relatively stable than Cr<sub>2</sub>O<sub>3</sub> on the alloy surfaces at high temperatures. Although the growth rates of Al<sub>2</sub>O<sub>3</sub> and Cr<sub>2</sub>O<sub>3</sub> on the alloys cannot be identified because the plots in Fig. 4 to 7 represent the weight changes that include the amounts of both oxide formation and oxide spallation, it is apparent that Cr<sub>2</sub>O<sub>3</sub> is more prone to spall, since after less oxidation cycles, the NiCr alloys exhibit significant weight loss. The oxidation test on a NiAl alloy coating showed that after exposed at 1050 °C for 1000 h, the alloy surface was covered with a large amount of Al<sub>2</sub>O<sub>3</sub>; the comparison of the alloy surface before and after the oxidation test is shown in Fig. 8 and 9. The white areas of the scanning electron microscope (SEM) image in Fig. 9a are Al<sub>2</sub>O<sub>3</sub>; the corresponding x-ray diffraction (XRD) spectrum in Fig. 9b confirms the presence of Al<sub>2</sub>O<sub>3</sub> on the alloy surface after the oxidation test.

### 4. Discussion

The simulation results show that the existing micromechanics-based model developed by Chan (Ref 23) can be used to predict cyclic oxidation behavior of NiAl and NiCr alloys where Al<sub>2</sub>O<sub>3</sub> and Cr<sub>2</sub>O<sub>3</sub> scales are referred to as protective layers with a good accuracy. One remarkable feature of this

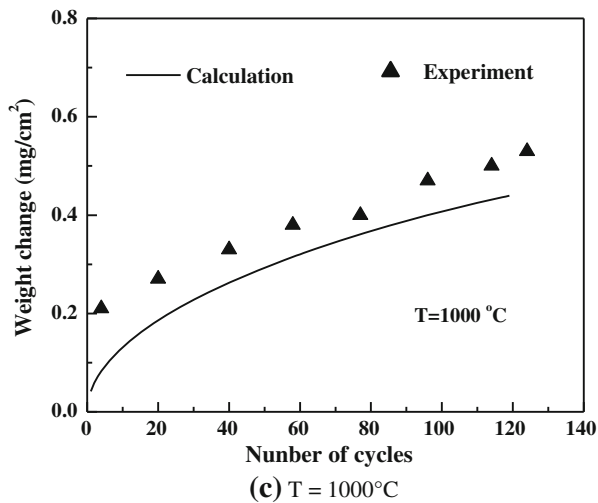
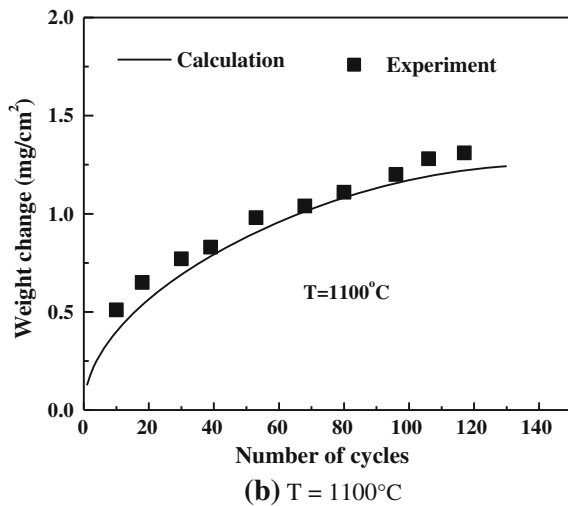
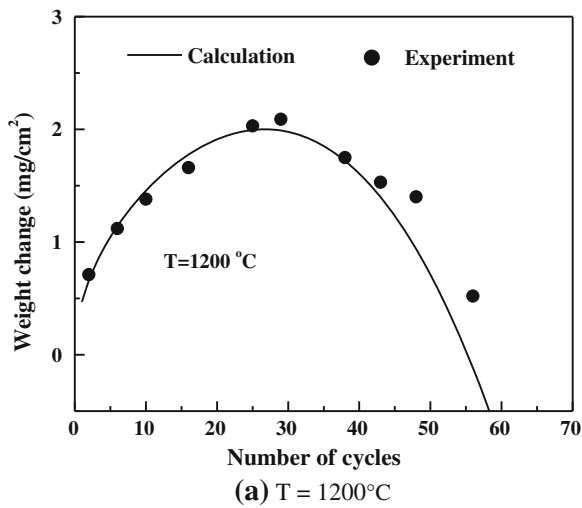


**Fig. 2** Cyclic oxidation and spallation of  $\text{Al}_2\text{O}_3$  on Fe-Ni-Cr-Al alloy steel (a) T = 1200 °C (b) T = 1100 °C (c) T = 1000 °C

model is that for any alloy or metal to be studied the so-called “complete” experimental cyclic oxidation curve must be obtained at a high temperature where the curve can have a maximum value of weight change, followed by a drop trend of

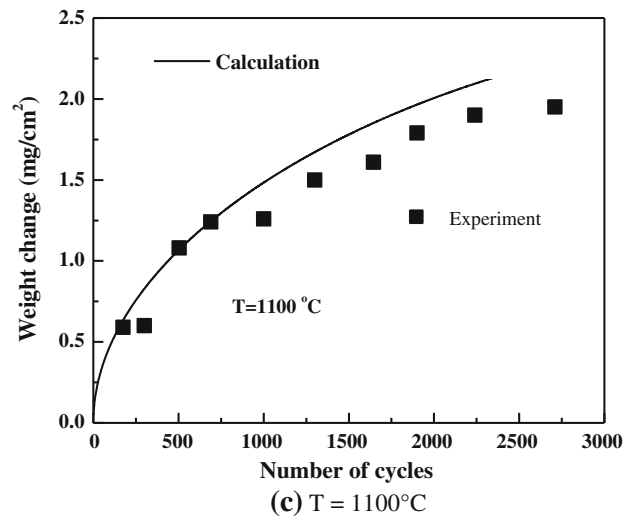
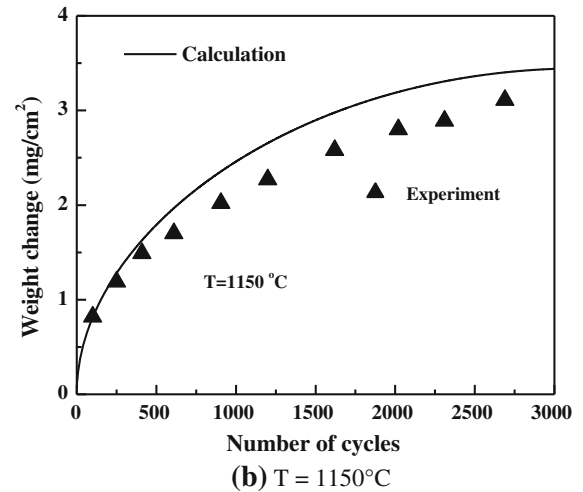
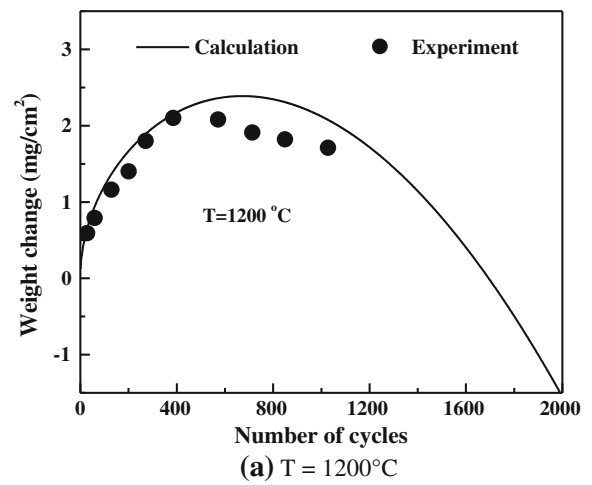


**Fig. 3** Cyclic oxidation and spallation of  $\text{Al}_2\text{O}_3$  on Ni-48.3Al-0.1Zr alloy (a) T = 1200 °C (b) T = 1150 °C (c) T = 1100 °C

weight change down to a zero point, before modeling, in order to determine the oxide crack density component,  $m$ , thus the oxide spallation constant,  $q$ . With this “complete” experimental cyclic oxidation curve, the model can predict the cyclic oxidation curves of the alloy or metal at other

**Table 2 Chemical Compositions (wt.%) of tested alloys**

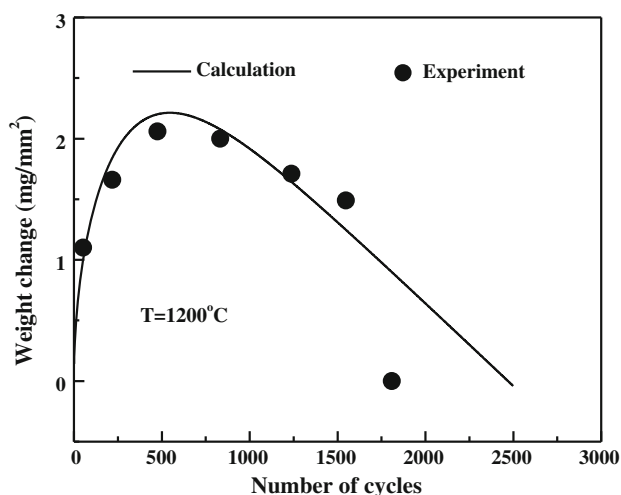
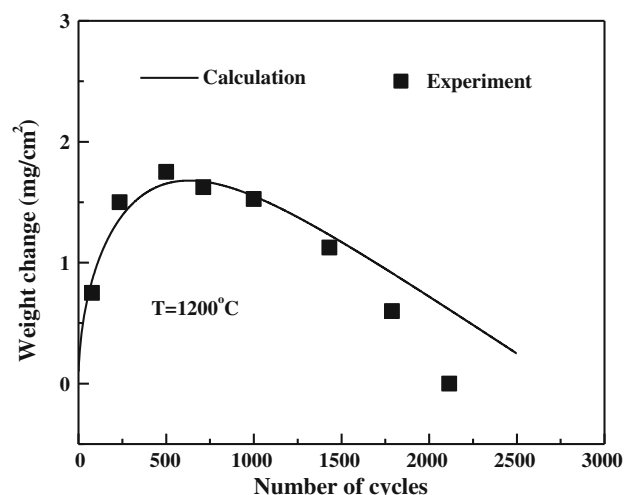
Material	Ni	Cr	Al	Fe
Ni-48Al-0.1Zr	Balance		48	
NiAl	Balance		31.5	
DH-245	Balance	20	3.5	0.7
Ni30Cr	Balance	30		

**Table 3 Calculated and revised  $m$  values for the tested alloys**

Material	Calculated $m$ value	Revised $m$ value	Error
Ni-48Al-0.1Zr	1.147	0.1	$(0.1-1.147)/1.147 = 91.3\%$
NiAl	0.042	0.01	$(0.01-0.042)/0.042 = 76.2\%$
DH-245	4.54	3.8	$(3.8-4.54)/4.54 = 16.3\%$
Ni30Cr	0.424	2	$(2-0.424)/2 = 78.8\%$

**Table 4 Parameters used in the cyclic oxidation simulation for the tested alloys**

Material	$T_{max}$ , °C	$T_{min}$ , °C	$K_p$ , $mg^2/cm^4/h$	$q$ , $mg/cm^2/°C^2$	$m$	$Z$	$t$ , h
Ni-48Al-0.1Zr	1200	25	0.02	$2.40 \times 10^{-10}$	0.1	2.125	1
NiAl	1200	25	0.01	$2.55 \times 10^{-10}$	0.01	2.125	1
DH-245	1150	25	0.056	$1.37 \times 10^{-11}$	3.8	3.167	1
Ni30Cr	1050	25	0.088	$1.15 \times 10^{-8}$	2	3.167	1

**Fig. 4** Weight change of Ni-48Al-0.1Zr alloy under cyclic oxidation at 1200 °C**Fig. 5** Weight change of NiAl alloy under cyclic oxidation at 1200 °C

different high temperatures. This is particularly beneficial for studying cyclic oxidation of materials at the temperatures lower than the temperature where the “complete” experimental cyclic oxidation curve is derived when economic issue is concerned, because at these temperatures, the cyclic oxidation test may take very long time to obtain the weight change curve that can depict the entire cyclic oxidation behavior of the materials at the temperatures, that is, the oxide scale experiences both growth and degradation steps. However, it should be noticed that it is not clear about the temperature range within which the  $m$  value can be considered constant. For the alloys Fe-Ni-Cr-Al and Ni-48.3Al-0.1Zr, within 1000-1200 °C, the same  $m$  values predicted reasonable cyclic oxidation curves, compared to the experimental measurements.

The most important application of the model is the prediction of cyclic oxidation of an alloy or metal at relatively low temperatures where it may take long time to obtain the entire experimental curves for the alloy or metal, for example, as shown in Fig. 2 and 3, for Fe-Ni-Cr-Al at the oxidation temperatures of 1100 and 1000 °C, after 140 cycles the weight reduction still does not happen yet, while at 1200 °C within 70 cycles, a “complete” cyclic oxidation curve with weight increase and decrease occurs. For Ni-48.3Al-0.1Zr, the time is even longer; at the oxidation temperatures of 1150 and 1100 °C, after 3000 cycles the weight still increases, and at 1200 °C a “complete” cyclic oxidation curve arrives after 2000 cycles. For this type of alloys, it is impossible to obtain the cyclic oxidation curve experimentally at the relatively low

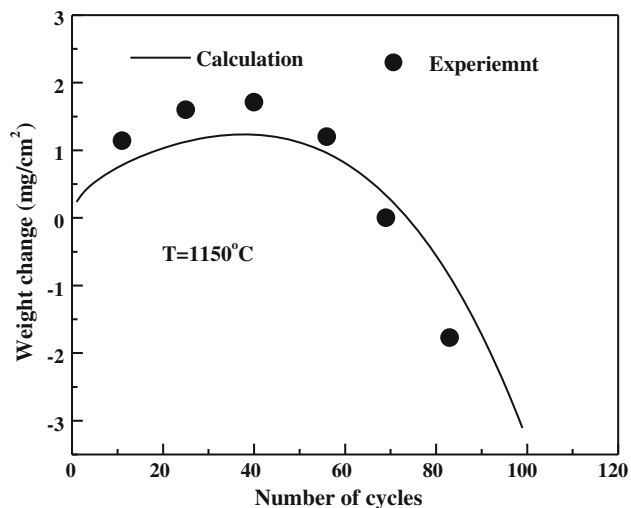


Fig. 6 Weight change of DH-245 alloy under cyclic oxidation at 1150 °C

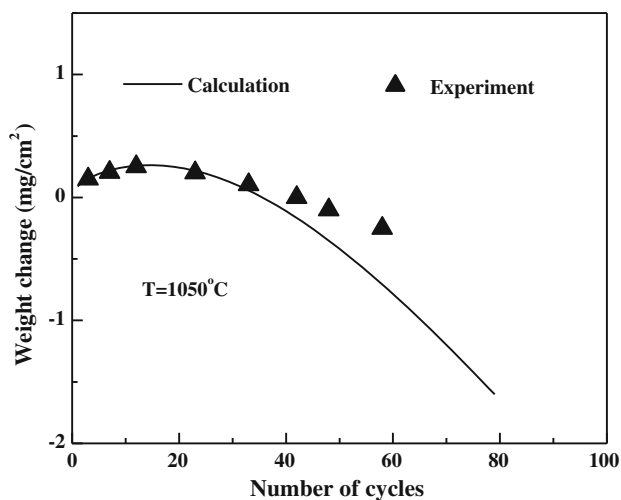
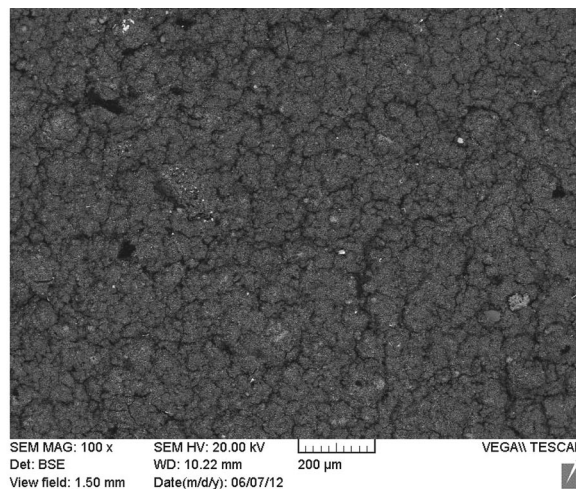


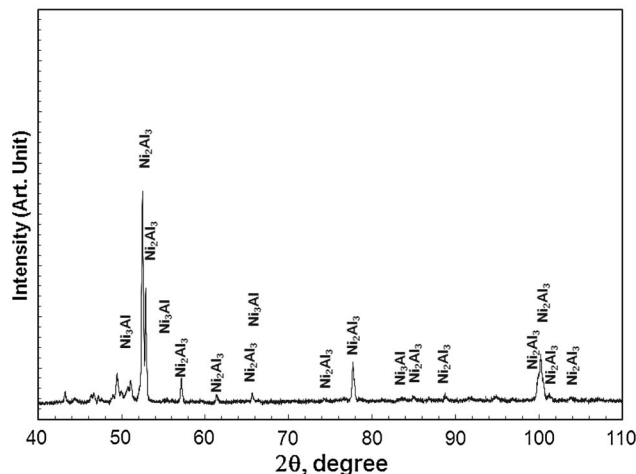
Fig. 7 Weight change of Ni30Cr alloy under cyclic oxidation at 1050 °C

temperatures, when time and cost are concerned. In this case, the micromechanics-based model being discussed exhibits its advantages.

In order to best fit the experimental data, the model parameter, oxide crack density exponent,  $m$ , is necessarily revised through a trial-and-error procedure as opposed to its initial evaluation expression, Eq 11. As shown in Table 3,  $\text{Cr}_2\text{O}_3$  as oxide protective scale on DH-245 has the least error in revising  $m$ . The error of  $m$  after revising for NiAl is 76.2%. For Ni30Cr, the error of  $m$  is 78.8% and for Ni-48Al-0.1Zr,  $m$  has the largest error of 91.3%. These large errors manifest that Eq 11 is almost invalid to determine the value of  $m$ . Therefore, it demonstrates that either oxide growth formulae or oxide spallation mechanism used in the Chan's model needs necessary modifications, and such work is under progress.



(a) SEM image of coating surface



(b) XRD spectrum of coating surface

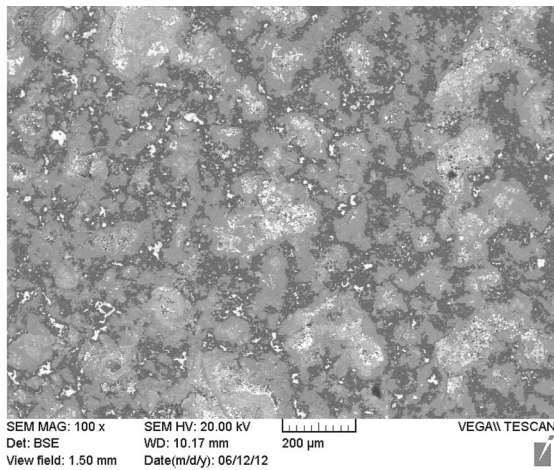
Fig. 8 NiAl alloy coating before high-temperature oxidation test (a) SEM image of coating surface (b) XRD spectrum of coating surface

## 5. Conclusions

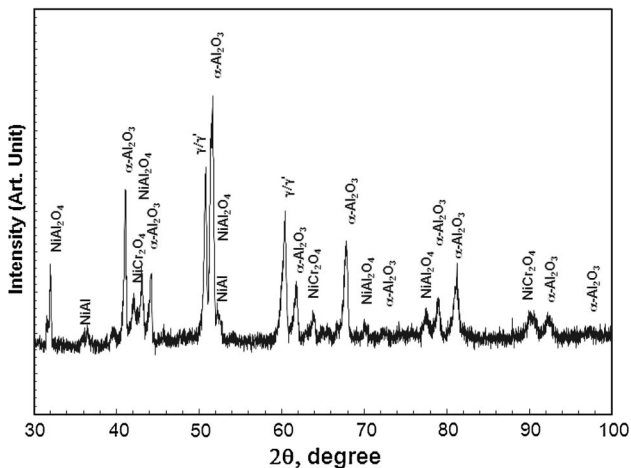
The micromechanics-based cyclic oxidation model given by Chan (Ref 23) was applied to study the cyclic oxidation behavior of four selected alloys, where either  $\text{Al}_2\text{O}_3$  or  $\text{Cr}_2\text{O}_3$  layer is formed as protective scales at high temperatures. A 'complete' weight change curve representing both oxide growth and spallation steps is necessarily required to derive the model parameters, with which the model can predict the oxidation behavior of the alloy at different temperatures.

The model parameter, oxide crack density exponent, needs to be revised through a trial-and-error procedure as opposed to its initial evaluation expression, in order to best fit the experimental data, and the errors are remarkable. Therefore, the theoretical equation for determining the parameter is almost invalid.

Comparing the cyclic oxidation behavior between NiAl and NiCr alloys, it is found that  $\text{Al}_2\text{O}_3$  is more stable than  $\text{Cr}_2\text{O}_3$  on the alloy surface at high temperatures, since  $\text{Cr}_2\text{O}_3$  is more prone to spall.



(a) SEM image of coating surface



(b) XRD spectrum of coating surface

**Fig. 9** NiAl alloy coating after exposed at 1050 °C for 1000 h (a) SEM image of coating surface (b) XRD spectrum of coating surface

## Acknowledgment

The authors are grateful for the financial support from Natural Science & Engineering Research Council of Canada (NSERC), the in-kind support from National Research Council Canada (NRC) and both financial and in-kind support from Kennametal Stellite Inc. Thanks are also given to Dr. Feng Gao, who has contributed to the oxidation test on a NiAl alloy coating and the SEM and XRD analyses of the coating surface before and after the test.

## References

1. F. Gao, Q. Yang, X. Huang, and R. Liu, Development of the Process Index for NiCrAlY Coatings with the Mettech Axial III™ System, *J. Mater. Eng. Perform.*, 2013, **22**(3), p 713–722
2. F. Gao, X. Huang, R. Liu, and Q. Yang, Optimization of Plasma Spray Process Using Statistical Methods, *J. Therm. Spr. Technol.*, 2011, **21**(1), p 176–186

3. T.Q. Liang, H.B. Guo, H. Peng, and S.K. Gong, Microstructural Evolution of CoCrAlY Bond Coat on Ni-Based Superalloy DZ 125 at 1050 °C, *Surf. Coat. Technol.*, 2011, **205**(19), p 4374–4379
4. M.P. Taylor, An Oxidation Study of an MCrAlY Overlay Coating, *Mater. High Temp.*, 2005, **22**(3-4), p 433–436
5. H.X. Hu, S.L. Jiang, Y.S. Tao, T.Y. Xiong, and Y.G. Zheng, Cavitation Erosion and Jet Impingement Erosion Mechanism of Cold Sprayed Ni-Al<sub>2</sub>O<sub>3</sub> Coating, *Nucl. Eng. Des.*, 2011, **241**(12), p 4929–4937
6. N. Voudouris and C. Christoglou, Angelopoulos GN Formation of Aluminide Coatings on Nickel by a Fluidised Bed CVD Process, *Surf. Coat. Technol.*, 2001, **141**, p 275–282
7. M. Haerig and S. Hofmann, Mechanisms of Ni<sub>3</sub>Al Oxidation Between 500 °C and 700 °C, *Appl. Surf. Sci.*, 1998, **125**(1), p 99–114
8. H.R. Guan, M.J. Li, and X.F. Sun, Evolution of Oxide Scale Morphology on (Ni, Pd)Al Coating During High Temperature Oxidation in Air, *Mater. Sci. Forum*, 2004, **461-464**(1), p 417–424
9. P. Berthod, Thermogravimetric Study of Oxide Spallation for Chromium-Rich Cast Cobalt-Based and Iron-Based Alloys Oxidized at High Temperature, *Open Corr. J.*, 2009, **2**, p 61–70
10. H.E. Evans, G.P. Mitchell, R.C. Lobb, and D.R.J. Owen, A Numerical Analysis of Oxide Spallation, *Proc. R. Soc. Lond. Ser. A*, 1908, **1993**(440), p 1–22
11. G.C. Wood, High-Temperature Oxidation of Alloys, *Oxid. Met.*, 1970, **2**(1), p 11–57
12. J. Robertson and M.I. Manning, Limits to Adherence of Oxide Scales, *Mater. Sci. Technol.*, 1990, **6**, p 81–91
13. M. Schütze, Mechanical Aspects of High-Temperature Oxidation, *Corr. Sci.*, 1993, **35**, p 955–963
14. M.M. Nagl and W.T. Evans, The Mechanical Failure of Oxide Scales Under Tensile or Compressive Load, *J. Mater. Sci.*, 1993, **28**, p 6247–6260
15. P. Hancock and J.R. Nicholls, Failure of Oxide Scales, *Mater. High Temp.*, 1994, **12**(2-3), p 209–218
16. H.E. Evans, Modelling Oxide Spallation, *Mater. High Temp.*, 1994, **12**(2-3), p 219–227
17. M. Schütze, An Approach to a Global Model of the Mechanical Behaviour of Oxide Scales, *Mater. High Temp.*, 1994, **12**(2-3), p 234–247
18. C.O. Moon and S.B. Lee, Analysis on Failures of Protective-Oxide Layers and Cyclic Oxidation, *Oxid. Met.*, 1993, **39**(1/2), p 1–13
19. J. Armitt, D.R. Holmes, M.I. Manning, D.B. Meadowcroft, and E. Metcalfe, The Spalling of Steam-Grown Oxide from Superheater and Reheater Tube Steels, *EPRI Report FP-686* (Palo Alto), Electric Power Research Institute, 1978
20. H.B. Probst, CE Lowell, Computer Simulation of Cyclic Oxidation, *J. Met.*, 1988, **40**(10), p 18–21
21. C.E. Lowell, C.A. Barrett, R.W. Palmer, J.V. Auping, and H.B. Probst, COSP: A Computer Model of Cyclic Oxidation, *Oxid. Met.*, 1991, **36**(1-2), p 81–112
22. C.A. Barrett, Effect of 0.1 at.% Zirconium on the Cyclic Oxidation Resistance of β-NiAl, *Oxid. Met.*, 1988, **30**(5-6), p 361–390
23. K.S. Chan, A Mechanics-Based Approach to Cyclic Oxidation, *Metall. Mater. Trans.*, 1997, **28A**, p 411–422
24. J.L. Smialek, J.A. Nesbitt, C.A. Barrett, and C.E. Lowell, Cyclic Oxidation Testing and Modelling: A NASA Lewis Perspective, *NASA/TM 209769* (Ohio), Glenn Research Center, 2000
25. H. Horii and S. Nemat-Nasser, Compression-Induced Microcrack Growth in Brittle Solids: Axial Splitting and Shear Failure, *J. Geophys. Res.*, 1985, **90**(B4), p 3105–3125
26. M.F. Ashby and S.D. Hallam, The Failure of Brittle Solids Containing Small Cracks under Compressive Stress States, *Acta Metall.*, 1986, **34**(3), p 497–510
27. V. Ramakrishnan, J.A. McGurty, and N. Jayaraman, Oxidation of High-Aluminium Austenitic Stainless Steels, *Oxid. Met.*, 1988, **30**(3-4), p 185–200
28. J.K. Doychak, The Evolution and Growth of Al<sub>2</sub>O<sub>3</sub> Scales on Beta-NiAl, *NASA Contractor Report 175097* (Ohio), 1986, p 1–239